





An Overview and Comprehensive Comparative Evaluation of Constant-Frequency Voltage Buck Control Methods for Series Resonant DC–DC Converters

VADIM SIDOROV  (Student Member, IEEE), ANDRII CHUB  (Senior Member, IEEE),
DMITRI VINNIKOV  (Senior Member, IEEE), AND ABUALKASIM BAKEER  (Student Member, IEEE)

Power Electronics Group, Department of Electrical Power Engineering and Mechatronics, Tallinn University of Technology, Tallinn 19086, Estonia

CORRESPONDING AUTHOR: DMITRI VINNIKOV (e-mail: dmitri.vinnikov@taltech.ee)

This work was supported in part by the Estonian Research Council under Grant PSG206, and in part by the Estonian Centre of Excellence in Zero Energy and Resource Efficient Smart Buildings and Districts, ZEBE, under Grant 2014-2020.4.01.15-0016 funded by the European Regional Development Fund.

ABSTRACT The paper focuses on galvanically isolated series-resonant dc-dc converters with a low quality factor of a magnetically integrated resonant tank. These converters can be controlled at a constant switching frequency to achieve the input voltage buck regulation. The paper compares various buck control methods, such as conventional pulse-width modulation, hybrid pulse-width modulation, shifted pulse-width modulation, hybrid shifted pulse-width modulation, improved shifted pulse-width modulation, asymmetrical pulse-width modulation, pulse-width modulation, and hybrid pulse-width modulation applied to the series-resonant dc-dc converter. The study considers step-up implementation of the series-resonant dc-dc converter topology with the voltage doubler rectifier, which makes it suitable as a front-end dc-dc converter for the integration of renewable energy sources in dc microgrids. The voltage buck control methods considered were compared analytically in terms of the cumulative power losses calculated theoretically. The theoretical results were compared with the experimental measurements to confirm the calculations and benchmark the voltage buck control methods. The experimental validation was performed using a 250 W prototype that demonstrated the hybrid PSM achieves the best performance. The experimental results were found in good agreement with analytically predicted values of the power loss.

INDEX TERMS Series resonant converters, dc-dc converters, pulse-width modulation, phase-shift modulation, dc microgrids.

I. INTRODUCTION

Sustainable development of humanity requires a wider use of electricity as a means of energy generation, transmission, and end-use [1]. Delay in widescale electrification would result in a technological barrier for economy that is net positive relative to the objectives of reduction of greenhouse emissions [2]. Wider adoption of renewable energy sources for electricity generation ensures low pollution and allows for adoption of highly decentralized or even autonomous power systems featuring high power supply security [3], [4]. The ongoing COVID-19 pandemic has proved the advantages of sustainable energy generation such as flexibility of energy

generation, high reliability, little need for maintenance, and no dependence on the supply of fossil fuels [5]. Cutting lifecycle costs of renewables is essential to achieve grid parity in most of countries, which is also associated with the reliability and cost of the power electronic systems [6].

Dc distribution is a promising technology that can improve the overall efficiency of renewable energy generation and distribution [7]. Dc microgrids will be the backbone of the future autonomous households and smart districts [8]–[10]. Considering that the renewable energy sources usually provide variable dc output voltage, the importance of the dc-dc converters cannot be overestimated. Currently, solar photovoltaic (PV)

energy is considered the main technology that can achieve the lifecycle cost low enough to ensure the market viability of the dc microgrids in the near future [11]. The best performance of the PV energy generation could be achieved using the module-level power electronics [12]. This application requires dc-dc converters with a wide input voltage range of up to one to six. The galvanically isolated buck-boost dc-dc converters (IBBCs) show the best performance in these applications [12]. Among them, the series resonant converter (SRC) topologies have attracted much attention of the researchers [13]. These topologies aim for magnetic integration of the resonant inductor to achieve high power density, which, however, results in operation at low quality factors of the resonant tank. This implementation of the resonant tank makes the SRC nearly insensitive to the conventional variable frequency control [15]. On the other hand, they can be controlled at a fixed switching frequency.

An SRC-based IBBC with a low quality factor operates as a dc transformer (DCX) at a certain voltage V_{th} when all semiconductor components are soft-switched. The boost mode at the constant switching frequency can be used at the input voltages (V_{in}) below the V_{th} , which requires an active or semi-active rectifier to step-up the voltage at the rectifier side using the resonant inductor as an ac boost inductor [14]. The buck mode is used at $V_{in} > V_{th}$ and requires a certain modulation method to be applied to the input-side transistors [16]–[18]. The boost control methods were proposed recently by applying circuits used in the power factor correction [13]. On the other hand, the buck control methods were known from late 1980s [15] and gained more attention in the last decade [16]. A generalized methodology for the analysis of the dc voltage gain has been presented in [16]. However, some of the existing buck control methods have not been analyzed systematically before.

The goals of this study are to overview, generalize, classify, and benchmark the constant frequency buck control methods for the SRC with low quality factor, which cannot be controlled with variable frequency modulation due to low sensitivity of the converter dc voltage gain to the switching frequency variations [15]. Employing these methods in the primary side of the converter, and constant frequency boost control methods in the active or semi-active secondary side enables SRC-based IBBC with a wide input voltage range. This study covers the conventional pulse-width modulation (PWM) [15], the hybrid PWM (HPWM) [16], the conventional phase-shift modulation (PSM) [17], [18], the hybrid PSM (HPSM) [19], [20], the shifted PWM (SPWM) [24], the hybrid shifted PWM (HSPWM) and the improved shifted PWM (ISPWM) [16], and the asymmetrical PWM (APWM) [21], [22]. The shifted PWM is excluded for brevity as it was proven in [16] that its hybrid and improved derivatives show better performance. The main contributions of this study are methodology for the calculation of power losses in the SRC and comprehensive benchmark of the constant-frequency buck control methods, which were verified experimentally for high step-up applications.

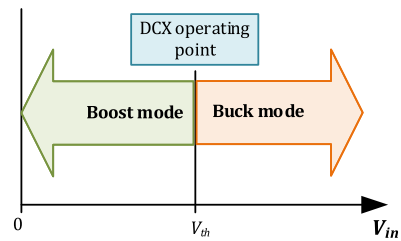


FIGURE 1. Arrangement of operating modes of an SRC-based IBBC.

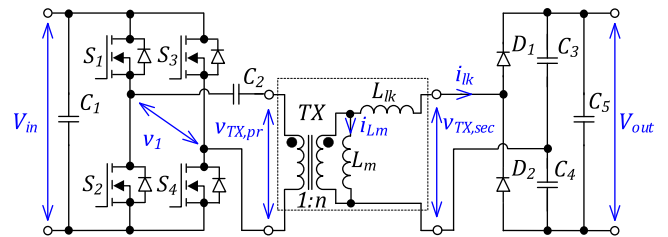


FIGURE 2. Topology of the series resonant converter under study.

This article is organized as follows. Section II of this article describes the SRC topology used in this study. Classification and generalized analysis methodology are

presented in Section III. Section IV provides a short description of the buck control methods. Next, Section V presents a systematic study of power losses for all considered buck control methods. In Section VI, the experimental waveforms are given to corroborate the idealized operating principle presented, and the measured power loss values are compared with those calculated theoretically. The results are discussed along with the future trends in Section VII. The last section draws conclusions.

II. DESCRIPTION OF SERIES RESONANT DC-DC CONVERTER

The topology of the high step-up SRC-based IBBC is shown in Fig. 2. It consists of the input-side full-bridge cell based on MOSFETs, an output side voltage doubler rectifier, an isolation transformer, and dc blocking capacitor in series with the transformer primary winding [23].

The angular resonant frequency of the resonant tank is defined as

$$\omega_r = \sqrt{\frac{1}{L_{lk}C_r}} \quad (1)$$

while the characteristic impedance is calculated as

$$Z_r = \sqrt{\frac{L_{lk}}{C_r}} \quad (2)$$

where L_{lk} is the leakage inductance of the transformer and C_r is equivalent resonant capacitance. The leakage inductance is considered as the only inductive element in the resonant tank. In general, the equivalent resonant capacitance the equivalent

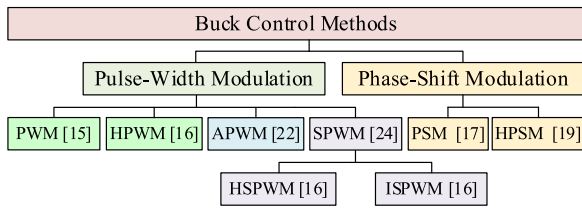


FIGURE 3. Classification of the buck control methods.

resonant capacitance considers influence of the blocking capacitor C_2 and output capacitors $C_3 - C_5$ as follows:

$$C_r = \frac{C_2 (C_4 C_5 + C_3 (C_4 + C_5))}{C_4 C_5 n^2 + (C_3 n^2 + C_2)(C_4 + C_5)} \quad (3)$$

The blocking capacitor neutralizes any dc bias current in the isolation transformer windings, which allows for the use of the asymmetrical control methods. Also, the capacitor allows for reconfiguration of the full-bridge switching cell into half-bridge. Typically, the capacitors C_2 and C_5 are dimensioned large enough to minimize their influence on the resonance. In such a case, the resonance frequency is defined mostly by the capacitors C_3 and C_4 , and the expression (3) for equivalent resonant capacitance could be simplified as $C_r = (C_3 + C_4)$.

In the considered case, the topology operates under the discontinuous resonant current mode. Hence, the switching frequency should be 5–10% below the resonant frequency to implement sufficient dead-time needed for soft-switching employing the transformer magnetizing current [24].

III. GENERALIZATION OF THE BUCK CONTROL METHODS

A. CLASSIFICATION

All buck control methods of the SRC operation with discontinuous current and fixed frequency are classified in Fig. 3. There are two main types of the buck control methods: the PWM and the PSM. The main difference between them is in duty cycle of the switches. In the PWM, the duty cycle of two or more transistors is variable, thus the voltage is controlled. In the PSM, the duty cycle of all transistors equals 0.5; the output voltage is controlled by the shift angle between the leading leg switches S_1, S_4 and the lagging leg switches S_2, S_3 . The PWM is subdivided into the classical PWM, the HPWM, the APWM, and the SPWM. The SPWM, in turn, is subdivided into the HSPWM and the ISPWM. In PWM methods, the duty cycle defines pulse width of switches. The PSM methods are subdivided into classical and hybrid PSM, where the duty cycle is a shift angle between the leading and lagging legs of the inverter. Section VI presents a detailed description of each method.

B. METHODOLOGY OF DC GAIN CALCULATION

An algorithm for deriving a closed-form expression of the dc voltage gain is demonstrated for the PWM methods of the SRC in [16]. This algorithm can be also applied for other buck control methods. The dc voltage gain of the converter normalized with respect to the transformer turns ratio n is

defined similar to [24]:

$$G = \frac{V_{out}}{2 \cdot n \cdot V_{in}} \quad (4)$$

The analysis of the circuit is based on the assumption of lossless components. An expression for the converter dc voltage gain can be derived using the power balance:

$$P_{in} = P_{out} \quad (5)$$

First, it is assumed that the input power equals the average power fed by the input-side inverter to the isolation transformer (ignoring the influence of the magnetizing inductance):

$$P_{in} = \frac{1}{T_{SW}} \int_0^{T_{SW}} v_1(t) \cdot n \cdot i_{lk}(t) dt \quad (6)$$

where v_1 is a piecewise-linear function of the input-side inverter voltage, i_{lk} is a piecewise function of the resonant current, T_{SW} is the switching period.

Output power is defined by the output voltage and the load as follows:

$$P_{out} = \frac{V_{out}^2}{R} \quad (7)$$

where V_{out} is the average output voltage and R is the load resistance.

Considering how (6)–(7) can be substituted into (5), the power balance can be represented as:

$$\frac{1}{T_{SW}} \int_0^{T_{SW}} v_1(t) \cdot n \cdot i_{lk}(t) dt = \frac{V_{out}^2}{R} \quad (8)$$

Taking into account (4), an equation of the converter dc gain can be derived from (8) analytically or numerically as a function of the converter parameters, duty cycle D_{SD} , and the input voltage:

$$G = f(V_{in}, D_{SD}, n, R, L_{lk}, C_r, T_{SW}) \quad (9)$$

This methodology is universal for all buck control methods considered in this paper. The only difference is how the time-functions of v_1 and i_{lk} are defined. A derivative example of the dc gain closed-form expression for the PWM, HPWM, and SPWM methods is presented in [16]. Similarly, closed-form expressions of dc gain for the APWM, PSM, and HPSM buck control methods can be calculated.

IV. DESCRIPTION OF BUCK CONTROL METHODS

This section focuses on the operation principle of the described methods. The methods were grouped into four based on the operation principle. In each method, the duty cycle is equal to a duration of voltage pulses applied to the resonant tank. The duty cycle controls the transferred energy through the resonant tank. Thus, the output voltage is controlled.

A. PWM AND HPWM

First, the PWM [15] is analyzed, which is the simplest buck control method for the full-bridge as well as the half-bridge application. The transistors in each leg of the input-side inverter are controlled with the same duty cycle and 180 degrees phase shift between the gating signals. As can be

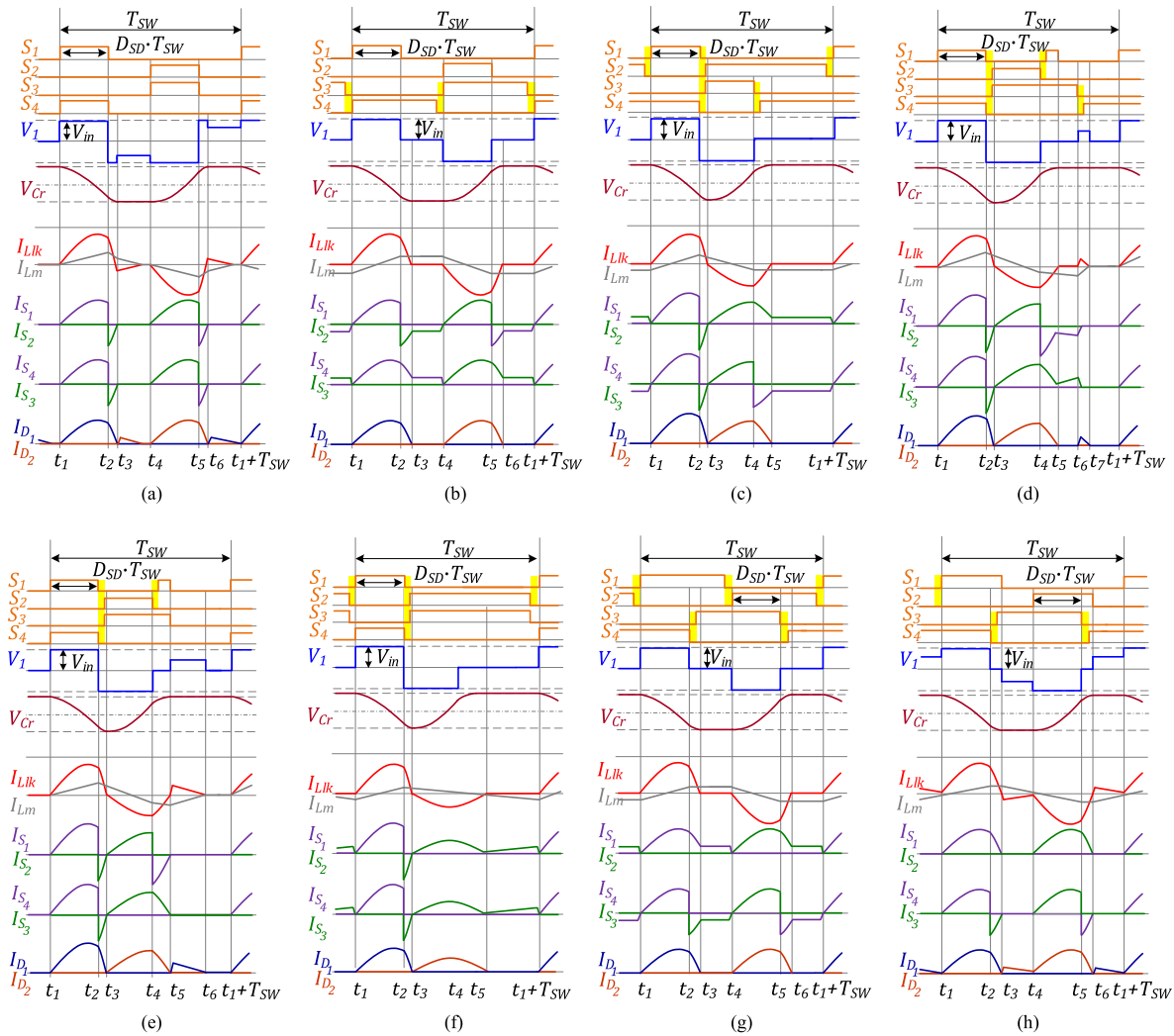


FIGURE 4. Idealized steady-state waveforms of the SRC controlled by the PWM (a), HPWM (b), SPWM (c), HSPWM (d), ISPWM (e), APWM (f), PSM (g), and HPSM (h).

seen from Fig. 4, the switches are turned on at zero current, but their turn-off is hard. When the transistors are turned off, the resonant current flows through the body diodes of MOSFETs. This is a significant drawback of this modulation method since transistors have high switching losses and the body diodes have high conduction losses and reverse recovery losses. At the instants t_3 , the currents of switches $I_{S1} \dots I_{S4}$ are equal to zero; however, the resonant current is equal to the magnetizing current of the transformer, which flows through the secondary side of the transformer and rectifier diodes (Fig. 4(a)). Thus, in this control method, the magnetizing current adds conduction and reverse recovery losses to the rectifier diodes.

The normalized gain of the PWM method can be calculated using the methodology (4)–(9)

$$G = \frac{1}{2} \left(B(1-A) - 1 + \sqrt{(B(A-1)+1)^2 + 4AB} \right) \quad (10)$$

This equation was first presented in [16]. There are three parameters used to simplify the equation:

$$A = C_r R f_{sw} \quad (11)$$

$$B = 1 - \cos(\omega_r D_{SD} T_{sw}) \quad (12)$$

where D_{SD} is the duty cycle of the active states of the front-end inverter. In the case of asymmetrical control, D_{SD} is the smaller of two duty cycles.

The hybrid PWM method was proposed in [16] to reduce the transistor switching losses and conduction losses of the body diodes. The duty cycle of switches S_3 , S_4 is always nearly 0.5, taking into account dead-time. This is the main difference from the PWM. These switches bypass their body diodes connected in parallel when the resonant current falls to zero. As can be seen from Fig. 4(b), only two transistors (S_1 and S_2) are turned off at a high current, other transistors are turned off at a low current, which is equal to the magnetizing current flowing through the transformer primary winding. It is because in this case, the magnetizing current flows through

the input-side bridge cell and influences the conduction and switching losses of the transistors. This method can be applied to control only the full-bridge cells, which is another difference from the PWM.

The normalized gain of the HPWM method is the same as the gain of the PSM method [17] and equals

$$G = \frac{1}{4} \left(B(1 - A) + \sqrt{B^2(A - 1)^2 + 8AB} \right) \quad (13)$$

B. SPWM, HSPWM AND ISPWM

The second group of the buck control methods is represented by various shifted PWM methods. As compared to the PWM, here, the control signals of the switches S_2 and S_3 are shifted in the vicinity of the control signal of the switches S_4 and S_1 ; they are separated by the dead-time. It is the main feature of each shifted method. As a result, the conduction losses in the MOSFETs body diodes are reduced because the switches S_2 , S_3 , and S_4 bypass their body diodes when the resonant current drops to zero at intervals $[t_2; t_3]$ and $[t_4; t_5]$ (Figs. 4(c)–4(e)). Switches S_2 , S_3 , and S_4 turn on at zero voltage, which would also reduce the switching losses, since their body diodes conduct during a short dead-time.

The voltage applied to the transformer and the output voltage are controlled by the duty cycle of S_1 and S_2 which are switched synchronously.

The SPWM demonstrated in [25] is similar to the modulation in [20]. Transistors operate complimentary with the dead-time. In the SPWM method, during the zero states of the inverter, when the resonant current is dropped to zero, two transistors S_2 and S_4 continue to conduct the magnetizing current. This feature increases conduction and switching losses in these MOSFETs since the magnetizing current is n times higher when it flows in the transformer primary winding compared to the secondary winding.

To avoid this drawback of the SPWM, the HSPWM was proposed in [16]. Ideal steady-state waveforms of the HSPWM are shown in Fig. 4(d). In the HSPWM, the zero state was eliminated by decreasing the duty cycle of the switch S_2 . The switch S_1 turns on again after the switch S_2 is turned off, which reduces the conduction losses as the body diode of the switch S_1 is bypassed. The second turn-on of the switch S_1 occurs at zero voltage after the dead-time, following the instant t_4 because the body diode is conducting. The switch S_1 is turned off at the instant t_5 when the resonant current is equal to zero. Switches S_3 and S_4 operate complimentary with the duty cycle nearly 0.5. During conduction of the switch S_3 , the magnetizing current flows through the input-side inverter, similar to the case of the SPWM. At the instant t_6 , when the switch S_3 is turned off, the magnetizing current stops flowing in the input side and starts flowing in the secondary side of the transformer. This effect adds switching losses in the MOSFETs.

Another modified version of the SPWM method is the ISPWM (Fig. 4(e)), which was also described in [16]. The main

difference from the HSPWM is in the duty cycles of switches S_3 and S_4 . The duty cycle of the S_4 equals the duty cycle of the switch S_1 . The switch S_3 conducts between the instants t_2 and t_5 when the resonant current is not zero. In this case, the magnetizing current flows only in the secondary side through the rectifier diodes.

The ISPWM and HSPWM can be used to control both the full-bridge and the half-bridge cells unlike the SPWM, which is used only to control the full-bridge cells.

The closed-form solution in a compact form was presented neither for the SPWM, HSPWM, and ISPWM methods nor for the PWM and the HPWM. Theoretical analysis of these shifted PWM method was performed using the numerical algorithm described in [16]. According to the power balance, the output voltage value can be found.

C. APWM

The APWM is another buck control method described and applied in [21], [22]. This method (Fig. 4(f)) can be applied to control both full-bridge and half-bridge cells. The positive part of the resonant current looks like in the previous modes; however, the negative part is always sinusoidal because the long conduction interval provides sufficient time for a complete sinusoidal half-wave. This improves the soft-switching performance of the converter. The voltages of the resonant tank and output voltage are controlled only by the duty cycle of switches S_3 and S_4 . There is also the zero state similar to the SPWM where the magnetizing current flows through the input-side MOSFETs and influences their conduction losses.

Taking into account (4)–(9), the normalized dc voltage gain of the SRC for the APWM method equals

$$G = \frac{1}{4} \left(B(1 - 2A) - 1 + \sqrt{(B(2A - 1) + 1)^2 + 16AB} \right) \quad (14)$$

Previously, only an explicit expression of the dc gain was provided for the SRC controlled with the APWM [21], [22]. The expression (14) is presented here for the first time.

D. PSM AND HPSM

The last group of the buck control methods is represented by the phase-shift control methods, i.e., the PSM and the hybrid PSM. These two methods can be applied to control only full-bridge cells.

Figure 4(g) shows the idealized waveforms of the SRC operating with the PSM. In this case, the voltage applied to the resonant tank is controlled by the phase shift angle between the leading-leg switches S_1 and S_2 , and the lagging-leg switches S_3 and S_4 . In each leg, complementary gating signals are applied to the switches. The phase shift angle defines the duration of the zero states in the input-side inverter when either top switches S_1 and S_3 or lower switches S_2 and S_4 conduct the magnetizing current (Fig. 4(g)). In addition, the conduction losses of the body diodes are eliminated because the switches S_3 and S_4 bypass the diodes. In the zero state, the

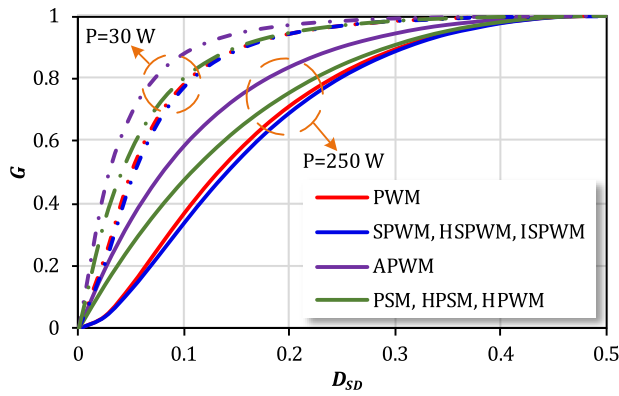


FIGURE 5. Theoretical normalized voltage gain of the case study SRC for PWM, HPWM, SPWM, HSPWM, ISPWM, PSM, and HPSM control methods.

resonant current drops to zero. In the PSM method, turn-off of two switches S_3 and S_4 is hard with the high resonant current and turn-off of the other two switches S_1 and S_2 is also hard but with low magnetizing current. The reason is that the magnetizing current flows through the primary windings of the transformer and the inverter. This increases conduction and switching losses in the transformer and MOSFETs.

The HPSM was proposed in [19] to improve the classical PSM control method. The zero states are avoided by decreasing the duty cycle of the switches S_1 and S_2 (Fig. 4(h)). As a result, when the resonant current equals zero, the magnetizing current stops flowing in the input side and starts flowing through the rectifier diodes.

The normalized dc voltage gain of the SRC for the PSM and the HPSM control methods corresponds to expression (13) first presented in [16].

E. COMPARISON OF GAINS

The normalized dc voltage gain of the case study converter calculated as a function of the duty cycle is plotted in Fig. 5 for two values of the operating powers, 30 W and 250 W, using (10)-(14) and the numerical analysis for the SPWM methods, as described in [16]. Table 1 presents the parameters used for the gain calculations. It could be appreciated from Fig. 5 that the described buck control methods have similar gain curves.

It is worth mentioning that each buck control method features a dead control zone, where the dc voltage gain G depends weakly on the duty cycle D_{SD} . When the load is changed, the Q -factor of the resonant tank is also changed. It has an impact on the voltage gain. Increase in the operating power results in the change of the dc voltage gain curve where the dead control zone is decreased.

As can be seen from Fig. 5, the gain curves of the PWM method are close to the curves of the SPWM, HSPM, and ISPWM. Accordingly, the gain (10) of the PWM can be used to calculate the theoretical normalized dc voltage gain for the SPWM method.

TABLE 1. Generalized Specifications of the Case-Study Converter

Operating parameters	
Input voltage, V_{in}	25...75 V
Output voltage, V_{out}	350 V
Switching frequency, f_{sw}	100 kHz
Operating power range	30...300 W
Components	
$S_1 \dots S_4$	On Semiconductor FDMS86180
D_1, D_2	CREE C3D02060E
C_1, C_5	150 μ F
C_2	52.8 μ F
C_3, C_4	38 nF
L_{lk}	35 μ H
L_m	1 mH
n	7.1

V. DERIVATION OF POWER LOSS MODELS

This section addresses a methodology for the calculation of power losses in the SRC. The methodology can help to understand the nature of power losses and compare buck control methods.

A. METHODOLOGY

Waveforms of the currents flowing through the resonant tank and switches as well as the shape of the resonant capacitor voltage are fairly similar for all the buck control methods (Fig. 4). The main difference lies in the time interval during which the resonant current decreases to zero. Nevertheless, the piecewise function of the resonant current can be defined as

$$i_{lk}(t) = \frac{v_1(t_i) \cdot n - v_{C_r}(t_{i-1}) - \Psi_{D_1}(t_i) \cdot V_{out}}{Z_r} \times \sin(\omega_r \cdot (t - t_i)), \quad (15)$$

where $v_1(t)$ is a piecewise function of the input-side inverter voltage, t_i is the i -th time instant, $\Psi_{D_1}(t)$ is a switching function of diode D_1 that can be written as

$$\Psi_{D_1}(t) = \begin{cases} 1, & \text{if } D_1 \text{ is conducting;} \\ 0, & \text{if } D_1 \text{ is off.} \end{cases} \quad (16)$$

The piecewise function of the resonant capacitor voltage could be defined as

$$v_{C_r}(t) = \frac{1}{C_r} \frac{di_{lk}(t)}{dt}. \quad (17)$$

At the same time, a piecewise-linear function of the magnetizing current equals

$$i_m(t) = \frac{(v_1(t_i) - v_{C_2}(t)) \cdot n}{L_m} \cdot \frac{t - t_{i-1}}{t_i - t_{i-1}} + i_m(t_{i-1}) \quad (18)$$

where $v_{C_2}(t)$ is an average voltage of the input-side resonant capacitor C_2 . In the symmetrical control methods, the average voltage is equal to zero. The calculation of the magnetizing

current assumes that each piece of the magnetizing current function is linear.

The three main (15), (17), and (18) define the current and the voltage of all circuit components.

Depending on the buck control method, the magnetizing current could flow through the primary or the secondary winding of the transformer, as can be seen from Fig. 4. Therefore, the current of the transformer primary winding equals

$$i_{TX,pr}(t) = \begin{cases} (i_{lk}(t) + i_m(t)) \cdot n; \\ i_{lk}(t) \cdot n. \end{cases} \quad (19)$$

By the same principle, the secondary side current of the transformer can be written

$$i_{TX,sec}(t) = \begin{cases} i_{lk}(t); \\ i_{lk}(t) - i_m(t). \end{cases} \quad (20)$$

From (19), currents of the input-side switches $S_1 \dots S_4$ are defined by the switching functions as follows:

$$i_{S_k}(t) = i_{TX,pr}(t) \cdot \Psi_{S_k}(t) \quad (21)$$

where k is the number of a switch, $\Psi_{S_k}(t)$ is a switching function of a switch, which is defined similar to (16).

In the same way, the currents of the rectifier diodes are defined

$$i_{D_j}(t) = i_{TX,sec}(t) \cdot \Psi_{D_j}(t) \quad (22)$$

where j is the number of a rectifier diode.

The input current of the inverter is

$$i_{in}(t) = i_{TX,pr}(t) \cdot \text{sign}(v_1(t)) \quad (23)$$

The output current of the voltage doubler rectifier is

$$i_{out}(t) = i_{D_1}(t) \quad (24)$$

It is assumed that ac components of the primary and secondary winding currents flow through the input capacitor C_1 and the output capacitor C_4 , respectively. An LCR bridge HAMEG HM8118 was used for the measurement of the winding equivalent resistances (ERs) of the magnetic components and resistances of a PCB.

The conduction losses of the MOSFETs, the transformer, the input and output capacitors are calculated using conventional methods, where each element is replaced with a corresponding resistor [26], [27]. For example, a drain-to-source resistance given in Table 2 represents a MOSFET in the on-state. ER of the transformer, the input and the output capacitors is imitating elements in AC with the switching frequency. Therefore, conduction power losses of these elements can be calculated as

$$P_{Cond(element)} = I_{RSM(element)}^2 \cdot R_{(element)} \quad (25)$$

Where $I_{RMS(element)}$ is the RMS current of an element, $R_{(element)}$ is an equivalent resistance of an element, which is shown in Tables II and III. It has to be taken into account that the input capacitor C_1 is a combination of SMD ceramic and film capacitors and the output capacitor C_5 is a combination of film and electrolytic capacitors. Also, the input and output resistance of a PCB was included in the power loss calculation. The equivalent input- and output-side resistances of a PCB are 5 mΩ and 3 mΩ, correspondingly.

TABLE 2. Datasheet Parameters of Semiconductor Components Used For Calculation of Losses

MOSFET On Semiconductor FDMS86180	
ON-state resistance	3.7 mΩ
Output capacitance	3250 pF
Gate-source voltage	9 V
Total gate resistance	3.5 Ω
Miller effects voltage	4.8 V
Rise time	12 ns
Fall time	7 ns
Gate-drain capacitance ($V_{DS}=0$ V)	530 pF
Gate-drain capacitance ($V_{DS}=35$ V)	68 pF
Body diode forward voltage	0.8 V
Body diode on resistance	28 mΩ
Body diode charge	109 nC
Diode Cree C3D02060E	
Forward voltage	0.8 V
On resistance	0.25 Ω
Total capacitance	10.5 pF
Total charge	120 nC

To calculate conduction losses in a body diode of a MOSFET or a rectifier diode, a diode is considered as a series connection of a voltage source and a resistance, imitating the forward voltage drop and the differential resistance of a diode [26]. Therefore, conduction power losses of a diode can be calculated as

$$P_{cond(diode)} = I_{rms(diode)}^2 \cdot R_{(diode)} + I_{av(diode)} \cdot V_f(diode) \quad (26)$$

where $I_{av(diode)}$ is the average current, $V_f(diode)$ is the forward voltage and $R_{(diode)}$ is the on-resistance of a diode. These parameters are listed in Table 2.

The calculation of switching losses in MOSFETs and diodes is based on the methodology from [27]. It uses the most conventional approach based on the datasheet parameters, such as parasitic output capacitance, fall and rise times, gate resistance and capacitance, etc.

The methodology of power losses calculation in a transformer core with non-sinusoidal waveforms is described in detail in [28]. An equation for power losses in a transformer core can be calculated as

$$P_{core} = \frac{V_e k_i (\Delta B)^{\beta-\alpha}}{T_{SW}} \sum_m \left| \frac{B_{m+1} - B_m}{t_{m+1} - t_m} \right|^\alpha (t_{m+1} - t_m) \quad (27)$$

where V_e is an effective volume of the core, k_i , α , β are Steinmetz coefficients determined by fitting of curves from the datasheet of the core material, B_m is the magnetic flux at

TABLE 3. Parameters of the Transformer and Capacitors Used For Calculation of Losses

Transformer RM14 3C95	
ER of windings	990 mΩ*
Primary turns	8
Secondary turns	50
μ _i	3000
Effective volume	13900 mm ³
Effective length	70 mm
Effective area	198 mm ²
α	1.045
β	2.44
k _i *	8.21
ESR of input and output capacitors	
ESR of C ₁ (f = 100 kHz)	9 mΩ
ESR of C ₅ (f = 100 kHz)	250 mΩ

*at 70°C

the instant t_m , ΔB is the peak-to-peak magnetic flux during the switching period T_{SW} .

The parameters of the transformer used for the calculation of the power losses are listed in Table 3. It has to be taken into account that the isolation transformer TX was implemented using RM14 core made of 3C95 ferrite material with an air gap of 0.6 mm, eight turns in the primary winding, and equivalent series resistance of 850 mΩ (at 25 °C) referred to the secondary winding [29], [30].

B. COMPARISON OF LOSS MECHANISMS

To benchmark the described buck control methods, current stresses have to be analyzed. Seven main current stresses were considered:

- RMS current of the MOSFET channel $I_{rms(S)}$ (considering current flowing only when a switch is turned on) - as it influences the conduction losses of the switches;
- average current $I_{av(bdS)}$ and the RMS current $I_{rms(bdS)}$ of the body diode (considering negative current flowing when a MOSFET is turned off) – as it could increase the conduction losses in the switches significantly;
- turn-off current $I_{off(S)}$ - as it defines the switching losses of the MOSFETs;
- RMS current of the transformer in the secondary side $I_{rms(TX,sec)}$ - as it influences the conduction losses of the transformer windings;
- RMS current of the rectifier diodes $I_{rms(in)}$ - as it influences the conduction losses of the rectifier diodes and the output-side capacitor;
- input RMS current $I_{rms(in)}$ - as it influences the conduction losses of the input-side capacitor;
- maximum current of the magnetizing inductance $I_{max(Lm)}$ - as it influences the conduction losses of the input-

TABLE 4. Current Stress of Elements At Vin = 35 V, P = 250 W for Different Buck Control Methods

Parameter	Value of current, A				
	PWM	HPWM	SPWM, HSPWM, ISPWM	APWM	PSM, HPSM
$I_{rms(S)}$	22.1	21.2	23.7	21.9	23
$I_{av(bdS)}$	3.5	4.1	0	0	0
$I_{rms(bdS)}$	8.9	8.9	0	0	0
$I_{off,max(S)}$	5.4	5.1	5.2	6.9	5.10
$I_{rms(TX,sec)}$	2.4	2.3	2.3	2.2	2.3
$I_{rms(D)}$	2.4	2.3	2.3	2.2	2.3
$I_{rms(Cin)}$	16.8	13.7	15.1	15.4	13.7

TABLE 5. Current Stress of Elements At Vin = 60 V, P = 250 W for Different Buck Control Methods

Parameter	Value of current, A				
	PWM	HPWM	SPWM, HSPWM, ISPWM	APWM	PSM, HPSM
$I_{rms(S)}$	24.9	22	28	24.5	26.4
$I_{av(bdS)}$	6.7	7.1	0	0	0
$I_{rms(bdS)}$	16	14.4	0	0	0
$I_{off,max(S)}$	8.8	6.9	8.5	9.5	6.9
$I_{rms(TX,sec)}$	2.9	2.6	2.7	2.4	2.6
$I_{rms(D)}$	2.9	2.6	2.7	2.4	2.6
$I_{rms(Cin)}$	20.9	11.8	16.4	17.3	11.8

or output-side components, which depends on the buck control method used.

The average current stress of the input and the output side is virtually the same for all the buck control methods and thus is excluded from the benchmarking. To compare symmetrical and asymmetrical control methods correctly, the cumulative RMS current of the MOSFETs was calculated as

$$I_{rms(S)} = \sqrt{\sum_{k=1}^4 I_{rms(S_k)}^2} \quad (28)$$

The RMS currents of the body diodes and the rectifier diodes were calculated in the same way. The average current of the body diodes is a sum of the average currents of each body diode.

These calculated steady-state current stresses for the studied control methods at points $V_{in} = 35$ V and $V_{in} = 60$ V at $P = 250$ W are shown in Tables 4, 5, and 6. The SPWM, the HSPWM, and the ISPWM methods have the same current

TABLE 6. Maximum Magnetizing Current At P = 250 W and Different Input Voltage for Different Buck Control Methods

Methods	$I_{max(L_m)}$, A	
	$V_{in}=35$ V	$V_{in}=60$ V
PWM	0.43	0.47
HPWM	0.22	0.18
SPWM	0.41	0.44
HSPWM	0.44	0.46
ISPWM	0.41	0.44
APWM	0.29	0.24
PSM	0.22	0.18
HPSM	0.39	0.35

TABLE 7. Features of The Buck Control Methods

Method	Transistors switched at high current	Number of conducting body diodes	Winding conducting the magnet. current
PWM	4	4	Secondary
HPWM	2	2	Primary
SPWM	3	0	Primary
HSPWM	3	0	Primary and secondary
ISPWM	3	0	Secondary
APWM	2	0	Primary
PSM	2	0	Primary
HPSM	2	0	Secondary

stress of the main components except for the maximum magnetizing current. For this reason, these methods, as well as the PSM and the HPSM methods, were grouped in one column. As shown in Tables 4 and 5, the PWM method has the highest current stress of elements (red values). Furthermore, the number of transistors switched at high current and the number of conducting body diodes is shown in Table 7. As can be seen from Table 7, the PWM has large amounts of switching transistors and conducting body diodes. Also, the body diodes of MOSFETs are conducting in the HPWM method, which is the main drawback of this method.

The PSM and the HPSM feature the lowest current stress and the smallest count of switching transients than other methods. Drawbacks of the shifted methods are the high RMS value of the current flowing in MOSFET channels (i.e., not taking into account MOSFET current flowing through the body diodes), three transistors switched at high current, and high magnetizing current (Table 6). In this case, it means that core losses of the transformer are increased as well as additional conduction losses in the converter caused by the

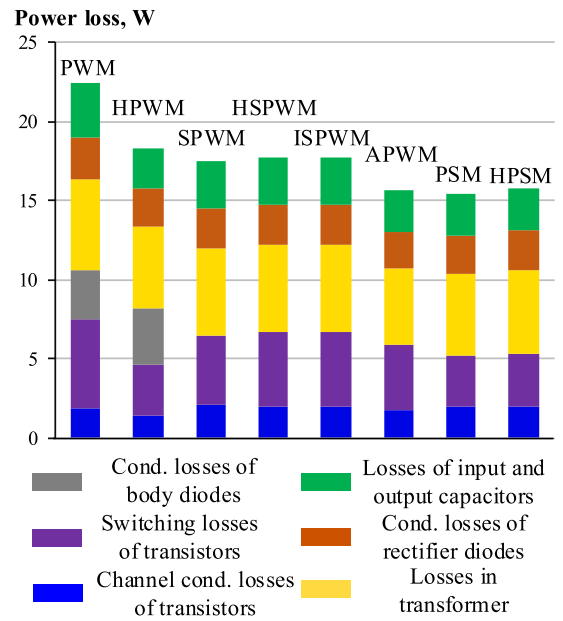


FIGURE 6. Diagram of power losses in the SRC at $V_{in} = 35$ V, $P = 250$ W for different buck control methods.

magnetizing current. The APWM method features moderate current stress and two transistors switched at high current, but as compared to other methods, these transistors are turned off at the highest current. It can be seen from Tables 4 and 5 that current stress in the circuit are increasing with increase of input voltage. This is mostly associated with decrease of the duty cycle D_{SD} , as can be seen from Fig. 5. However, the same trend among current stresses is observed in Table 5 when compared to Table 4.

Table 7 also shows the side(s) where the magnetizing current flows during the switching period. In the case when the magnetizing current flows in the input side, it increases the conducting losses in the primary winding of the transformer and MOSFETs as well as the switching losses in MOSFETs. Therefore, in the other case, the magnetizing current adds conducting losses in the secondary winding of the transformer and the rectifier diodes. It should be noted that the magnetizing current flowing in the primary winding of the transformer is n times higher than in the secondary winding. Therefore, the magnetizing current flowing in the secondary winding is less harmful for the converter efficiency compared to when it flows in the primary winding.

Power losses calculated at $V_{in} = 35$ V and $P = 250$ W based on the described methodology are shown in Fig. 6. The bar chart includes conduction losses of transistors (blue), switching losses of transistors (magenta), conduction losses of body diodes (gray), conduction losses of the transformer windings (yellow), conduction losses of rectifier diodes (orange), and combined losses of input and output side components (green). These losses are dominant in the given converter. All buck control methods feature nearly equal but low conduction losses of transistors. This results from using high-performance

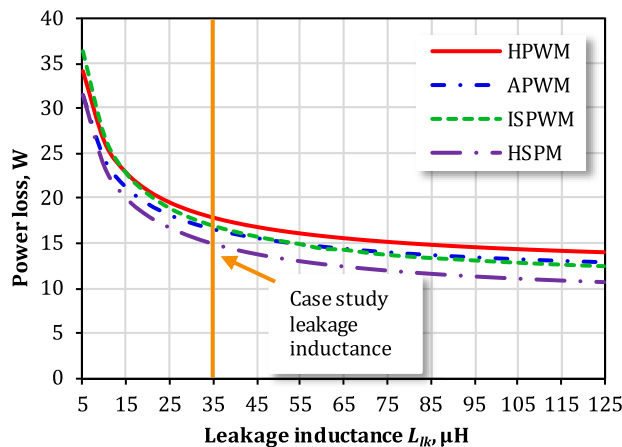


FIGURE 7. Dependence of losses on the leakage inductance.

MOSFETs with low on-state resistance. The main difference is in the duty cycle deviations and the magnetizing current path in the circuit, which also influences the transformer and rectifier diodes losses. Different magnetizing current values influence the transformer losses that consist of the copper losses and the core losses.

The PWM and HPWM feature conduction losses of the body diodes, which is a significant drawback. They would result in increased temperatures of transistors and should be taken into account in the converter thermal design.

The main drawback of the SPWM and PWM method is high switching losses. The reason revealed in Table 7 is that a large number of transistors are turned off at high current in comparison with other methods. The APWM and two PSM methods have a nearly equal total power loss. However, in the case of the APWM, transistor switching losses and losses of input and output capacitors are higher in comparison with PSM methods, while conduction losses of transistors and the transformer are higher in the PSM methods. This aspect would result in increased temperatures of these two MOSFETs and should be taken into account during the thermal design of the converter.

An amplitude of the resonant current influences directly all types of power losses. As can be seen from (15), the amplitude depends inversely on the impedance of the resonant tank (3), which is dependent directly on the leakage inductance. The dependence of total losses on the leakage inductance for four high-performance methods at $V_{in} = 35$ V, $P = 250$ W is summarized in Fig. 7. These four curves feature virtually the same shape. With the inductance increasing, total losses are decreasing. Above $50 \mu\text{H}$, the total losses are weakly dependent on the inductance. In the case study converter the transformer with the internal leakage inductance $35 \mu\text{H}$ was used. This is the maximum value of the internal leakage inductance for this transformer type. The difference in the power losses between values $35 \mu\text{H}$ and $100 \mu\text{H}$ is about 4.5 W. However, the values of more than $50 \mu\text{H}$ can be achieved by an external inductor, which, however, increases the conduction losses, cost, size, and weight of the converter.

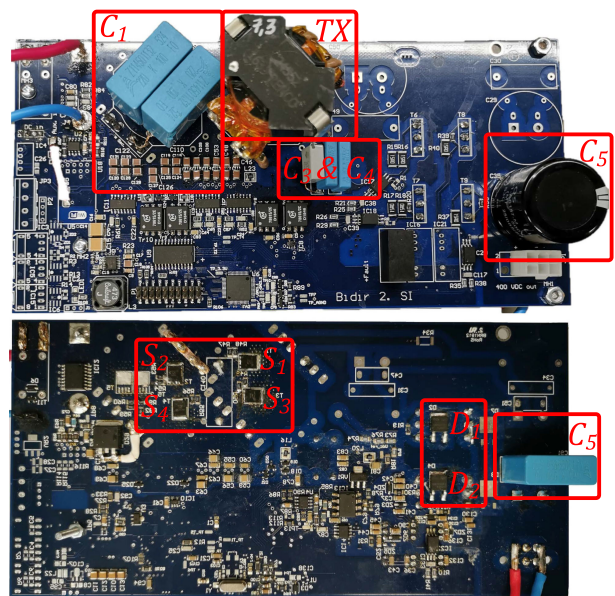


FIGURE 8. Experimental prototype of the series resonant converter.

VI. EXPERIMENTAL RESULTS

A prototype of the SRC converter was built to verify the operation of the buck control methods and compare experimental results with the theoretical methodology. The main specifications of the prototype are listed in Table I. The prototype is shown in Fig. 8.

A. STEADY-STATE WAVEFORMS

Voltage and current waveforms of the SRC operating in PWM, HPWM, APWM, SPWM, HSPWM, ISPWM, PSM, and HSPM control methods at $V_{in} = 35$ V, $P = 250$ W are shown in Fig. 9. The following measurement equipment was used: oscilloscope Tektronix DPO7254, differential voltage probes Tektronix P5205A, current probes Tektronix TCP0030A, and a precision power analyzer Yokogawa WT1800.

The measured waveforms of transformer current (Fig. 9) correspond to the theoretical curve of the resonant current in Fig. 4 for each buck control method. However, in the case of PWM, HSPWM, ISPWM, and HSPM, the voltage shape of the transformer primary winding has a parasitic oscillation between the output capacitances of semiconductor devices and the leakage inductance (Fig 9(a), 9(e), 9(f), and 9(h)). In the cases of HPWM, APWM, SPWM, HSPWM, and PSM, the secondary transformer voltage has a parasitic oscillation between the junction capacitances of the rectifier diodes and the leakage inductance (Fig. 9(b), 9(c), 9(d), and 9(g)). The HSPWM method features parasitic oscillations after the transistor S_3 is turned off and S_4 is turned on after a short dead-time (Fig. 9(e)). In the case of the ISPWM method, there are parasitic oscillations between the output capacitances of the semiconductor components and the magnetizing inductance of the transformer (Fig. 9(f)). All the described parasitic oscillations occur when the resonant current drops to zero.

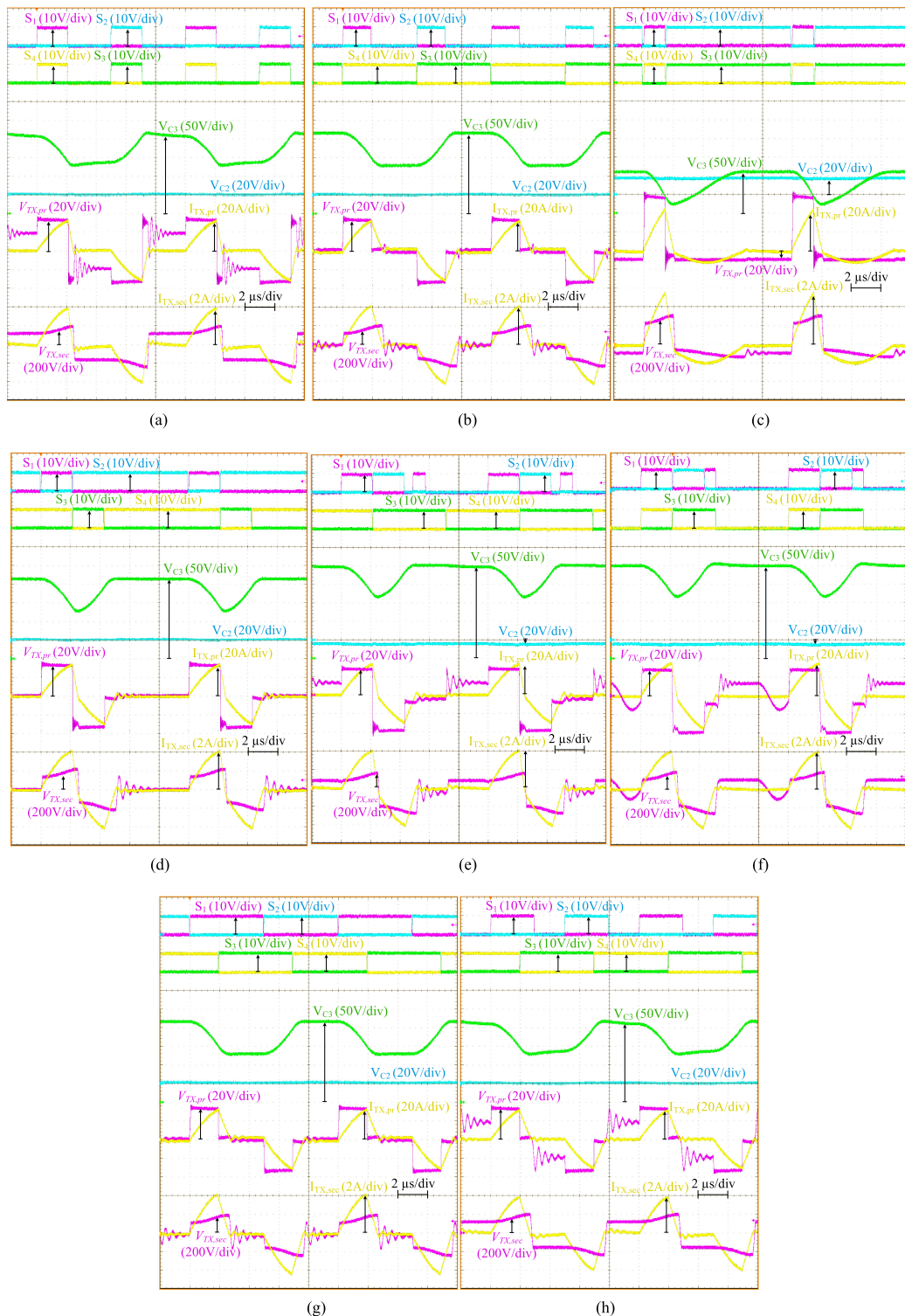


FIGURE 9. Experimental steady-state waveforms of the SRC operating at $V_{in} = 35$ V, $P = 250$ W for PWM (a), HPWM (b), APWM (c), SPWM (d), HSPWM (e), ISPWM (f), PSM (g), and HPSM (h) buck control methods.

These oscillations add extra conduction losses in the transformer and semiconductor devices.

As can be seen from Fig. 9, the voltage of capacitor C_3 is changing when the resonant current is equal to zero in PWM, HSPWM, ISWPM, and HPSM methods. It is the result of the

magnetizing current flowing in the secondary winding of the transformer.

The magnitudes of the transformer current depend on the quality factor of the resonant tank, the turns ratio of the transformer, and the load power. Therefore, the magnitudes

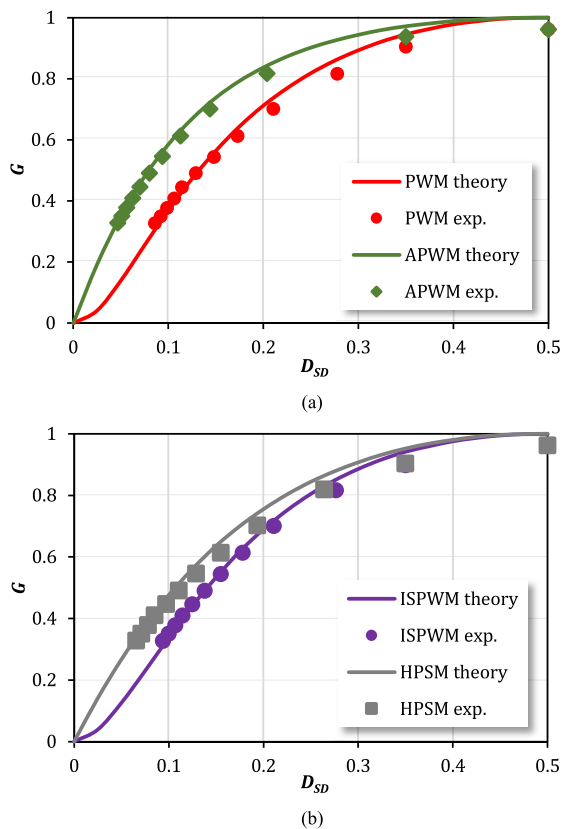


FIGURE 10. Normalized voltage gain of the case study SRC for PWM and APWM (a), ISPWM and HPSM (b) at $P = 250$ W.

of the transformer current are practically the same for some modulation methods. But their magnitude is the highest for the APWM method, as described in Section V.

B. COMPARISON OF EXPERIMENTAL AND THEORETICAL CONTROL VARIABLES

Experimental and theoretical values of the normalized dc voltage gain of the case study converter were plotted for the PWM, APWM, ISPWM, and the HPSM methods as a function of the duty cycle D_{SD} in Fig. 10. At the same time, Fig. 11 presents the duty cycle D_{SD} as a function of the input power for the same methods. Hereinafter, in figures, solid lines correspond to the theoretical values, while dots present experimental data. Theoretical curves in Figs. 10 and 11 were obtained using (10), (13), (14), and the numerical analysis for the ISPWM described in [16]. They are compared to the experimental results for the input voltage range from 25 V to 75 V (Fig. 10) and for the input power range from 30 W to 300 W (Fig. 11). It can be seen from the figures that the voltage gain curves are almost identical for all the compared methods. The four methods considered in Figs. 10 and 11 show good agreement between the theoretical and experimental results. It is worth mentioning that the experimental values of the duty cycle D_{SD} for PWM and ISPWM are virtually identical, which proves the assumption of equivalence of their dc gain curves made

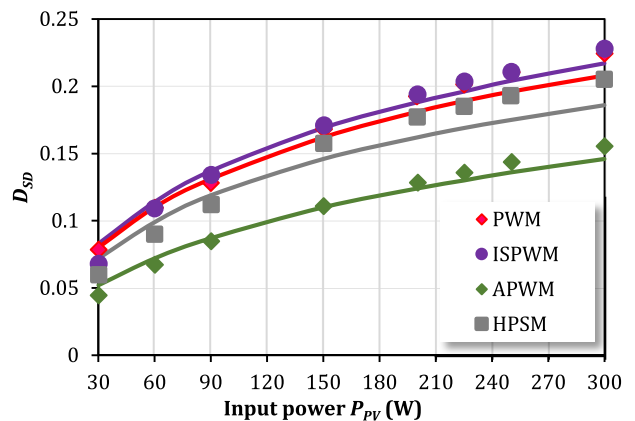


FIGURE 11. Duty cycle of the case study SRC for PWM and APWM (a), ISPWM and HPSM (b) at $V_{in} = 35$ V and different power.

in [16]. Small differences between theoretical and experimental values occur outside the target regulation range and are mostly associated with the assumptions of a lossless system, neglecting the influence of the magnetizing inductance during the analysis. As can be seen from Fig. 5, other reviewed methods have theoretical gain curves that coincided with those for the four selected methods. Therefore, other methods were omitted from Figs. 10 and 11 for better clarity and readability.

C. COMPARISON OF EXPERIMENTAL AND THEORETICAL POWER LOSSES

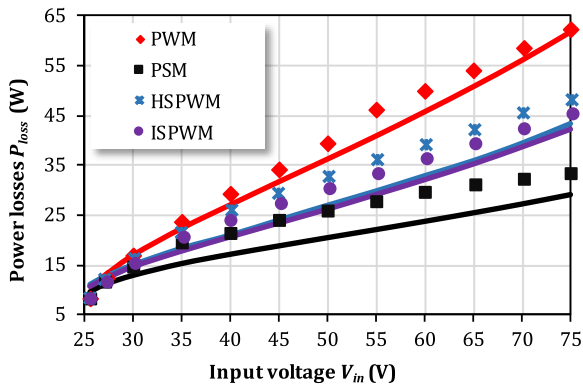
Figures 12 and 13 show the results of the calculation of theoretical power losses (solid lines) based on the described methodology in comparison with experimental losses (markers) for all buck control methods at $P = 250$ W and different input voltages (Fig. 12), at $V_{in} = 35$ V and a different power (Fig. 13), respectively. Increasing the input voltage increases the power losses since the duty cycle is decreased. With increased power, the resonant current and the duty cycle are increased. Therefore, the resonant current influences conduction losses in the elements and switching losses of the transistors.

As can be seen from Figs. 12 and 13, the methodology described in Section V shows good agreement with the experimental results. Thereby, this methodology can be used in the future research work. Deviations between the theoretical and experimental results are mostly associated with uncertainties and temperature drift of the datasheet parameters, and parasitic power losses in a PCB.

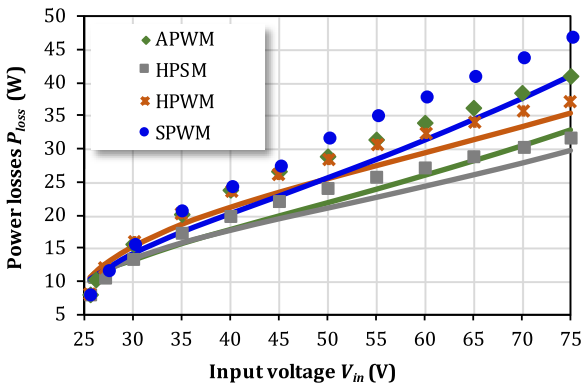
D. EFFICIENCY

Efficiencies of the prototype as a function of the input voltage and as a function of power for different control methods are shown in Fig. 14.

The maximum efficiency of the prototype equals 96.7% at $V_{in} = 25$ V, $P = 250$ W, $D_{DS} = 0.5$ for all control methods. This is a point of the maximum dc voltage gain. At this point, switches are turned on and off at zero current because the resonant current is virtually sinusoidal. With an increase of



(a)



(b)

FIGURE 12. Power losses of the converter for PWM, PSM, HSPWM, ISPWM (a); APWM, HPSM, HPWM, SPWM (b) at $P = 250$ W.

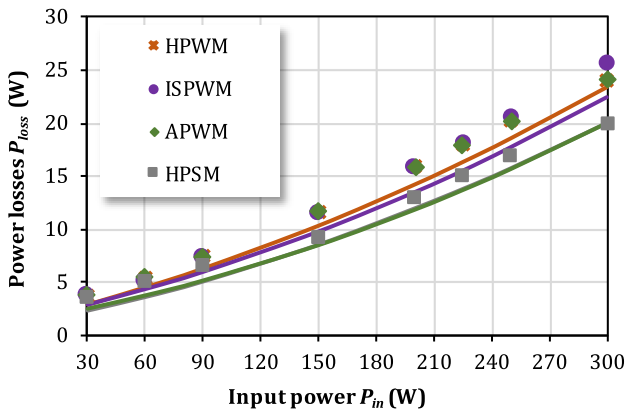
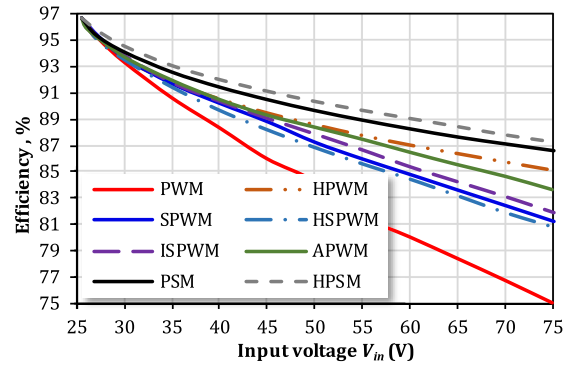


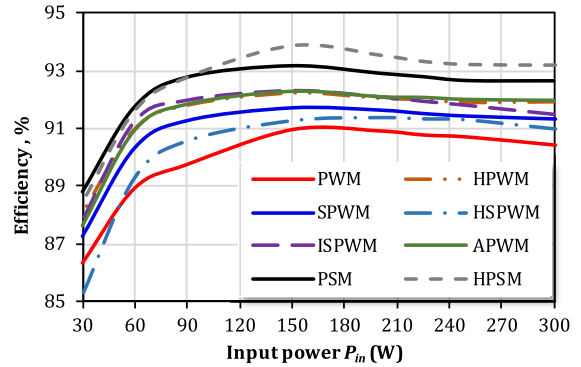
FIGURE 13. Power losses of the converter for HPWM, ISPWM, APWM, HPSM at $V_{in} = 35$ V.

the input voltage, the duty cycle decreases, thus increasing the power losses. The difference in the efficiency is mostly associated with the conduction losses in the body diodes of the MOSFETs, switching losses in the transistors, and power losses from the magnetizing current. In each control method, the efficiency is decreased at a low power range since the transformer core losses from the magnetizing current and parasitic oscillation prevail over other types of losses.

The HPSM has the highest efficiency at different voltages and different powers. The main difference of the efficiency



(a)



(b)

FIGURE 14. Efficiency of the case study SRC at $P = 250$ W and different voltage (a); at $V_{in} = 35$ V and different power (b).

between the PSM and the HPSM is associated with the difference in the conduction losses resulting from the magnetizing current flowing through different converter components and the parasitic oscillations, as it was described in Section VI. The number of transistors switched at high current is also two in the APWM and the HPWM methods as well as in the PWM and the HPSM. However, as Table 4 shows, the APWM features the highest amplitude of the switching current and the HPWM has high conduction losses of body diodes. The efficiency curves of the shifted methods are close to each other. The differences of these curves are caused by influence of the parasitic oscillation and the transformer magnetizing current that flows through different converter components. The main drawback of this method is the cumulative switching losses of transistors in comparison with the previous four methods. The PWM has the lowest efficiency. When using the PWM control methods, all transistors are turned off at high current, which results in the dominance of the switching losses.

VII. DISCUSSION OF RESULTS AND FUTURE RESEARCH

This paper focuses on the comparison of the buck control methods to control the SRC. Eight different methods were described in detail. For a comprehensive comparison of these methods, the methodology of power loss calculation was proposed. This methodology is based on the calculation of current and conduction and switching power losses in the used elements of the circuits, such as transistors, body diodes of

MOSFET, rectifier diodes, the transformer, input and output capacitors, input and output resistance of the PCB. Also, the methodology involves the calculation of normalized dc voltage gain.

As can be seen from the experiments, theoretical calculation of the dc voltage gain and power losses based on the methodology are in good agreement with experimental results. However, there are small deviations between the calculated and measured values. In the case of the dc voltage gain, small differences are mostly associated with the assumptions of a lossless system. In the case of power losses, reasons for deviations are parameter drift of circuit elements, variation in the operating temperature of the elements, conduction, and parasitic losses in the PCB. Also, it should be noted that copper losses of the transformer were calculated as conduction losses in the ER of the primary and secondary windings, which was referred to the secondary winding only for simplicity. The magnetizing current usually flows only in one of the windings. This depends on the control method (Table 6). Therefore, the estimation of the transformer copper losses is either slightly overestimated or underestimated. This is a minor drawback of the proposed methodology. In any case, transformer losses prevail over other losses in the built prototype. Future research should address the design of a high-efficiency transformer with high leakage inductance for the SRC as the conventional designs usually result in high ac resistance caused by high proximity losses in the secondary winding of the step-up transformer.

In summary, comparison of the buck control methods shows that the hybrid PSM is the best performing buck control method for the SRC converter. However, the HPSM cannot be used to control a half-bridge converter. Only the PWM, the ISPWM, and the APWM can be used for both full- and half-bridge converters. The results of the comparison between these methods showed that the APWM has high efficiency at different input voltages and different power levels.

It should be noted that in the APWM, two transistors have high switching current; therefore, they have high switching losses and, consequently, higher junction temperature. Thus, the feasible input voltage could be limited. This aspect should be taken into account during the thermal design of the converter.

The other control methods have one, two, or more drawbacks mentioned above, which increases the power losses in the converter. Future research will focus on a synthesis of new control methods based on optimal use of the existing methods and transition between them to achieve high efficiency within a wide input voltage range, which would further extend the converter operating range.

VIII. CONCLUSION

The paper has compared the buck control methods applied to the SRC with the discontinuous resonant current and fixed frequency. This study targets applications with high input current and low input voltage. Eight existing control methods were considered in detail. A methodology of power loss

calculation was proposed for the benchmarking. As the experiments demonstrated, the theoretical calculations based on the proposed methodology showed a good compliance with the experimental results. However, a drawback of the methodology is related to the theoretical transformer model. Future research will focus on improving this model.

In summary, the theoretical and experimental comparisons of the buck control methods revealed the HPSM as the best performing buck control method for a full-bridge SRC. It was also found that the APWM is the best buck control method for a half-bridge SRC.

As the analysis of the control methods showed, the main drawback of the SRC with a low-quality factor is in the operation at low duty cycle values, resulting in high RMS current stress of the components, which deteriorates the converter efficiency. Nevertheless, two directions of efficiency improvement could be suggested for the future research: analysis of soft-switching implementation possibilities to reduce the switching losses, optimization of the transformer design to reduce the equivalent resistance of the windings, which causes high conduction losses while keeping relatively high leakage inductance of the transformer.

REFERENCES

- [1] R. Jones, B. Haley, G. Kwok, J. Hargreaves, and J. Williams, "Electrification and the future of electricity markets: Transitioning to a low-carbon energy system," *IEEE Power Energy Mag.*, vol. 16, no. 4, pp. 79–89, Jul./Aug. 2018.
- [2] K. Dennis, "Environmentally beneficial electrification: Electricity as the end-use option," *Electricity J.*, vol. 28, no. 9, pp. 100–112, Nov. 2015.
- [3] S. V. Valentine, "Emerging symbiosis: Renewable energy and energy security," *Renewable Sustain. Energy Rev.*, vol. 15, no. 9, pp. 4572–4578, Dec. 2011.
- [4] F. Gökgöz and M. T. Güvercin, "Energy security and renewable energy efficiency in eU," *Renewable Sustain. Energy Rev.*, vol. 96, pp. 226–239, Nov. 2018.
- [5] V. Castán Broto and J. Kirshner, "Energy access is needed to maintain health during pandemics," *Nat. Energy*, vol. 5, no. 6, pp. 419–421, May 2020.
- [6] Z. Xin-gang, L. Pei-ling, and Z. Ying, "Which policy can promote renewable energy to achieve grid parity? Feed-in tariff vs. renewable portfolio standards," *Renewable Energy*, vol. 162, pp. 322–333, Dec. 2020.
- [7] M. Stieneker and R. W. De Doncker, "Medium-voltage DC distribution grids in urban areas," in *Proc. PEDG*, Vancouver, BC, 2016, pp. 1–7.
- [8] D. L. Gerber, V. Vossos, W. Feng, C. Marnay, B. Nordman, and R. Brown, "A simulation-based efficiency comparison of AC and DC power distribution networks in commercial buildings," *Appl. Energy*, vol. 210, pp. 1167–1187, Jan. 2018.
- [9] A. Chub, D. Vinnikov, O. Korkh, M. Malinowski, and S. Kouro, "Ultra-Wide voltage gain range microconverter for integration of silicon and thin-film photovoltaic modules in DC microgrids," *IEEE Trans. Power Electron.*, to be published.
- [10] V. Vossos, D. Gerber, Y. Bennani, R. Brown, and C. Marnay, "Techno-economic analysis of DC power distribution in commercial buildings," *Appl. Energy*, vol. 230, pp. 663–678, Nov. 2018.
- [11] S. Comello, S. Reichelstein, and A. Sahoo, "The road ahead for solar PV power," *Renewable Sustain. Energy Rev.*, vol. 92, pp. 744–756, Sep. 2018.
- [12] D. Vinnikov, A. Chub, E. Liivik, R. Kosenko, and O. Korkh, "Solar Optiverter—A novel hybrid approach to the photovoltaic module level power electronics," *IEEE Trans. Ind. Electron.*, vol. 66, no. 5, pp. 3869–3880, May 2019.
- [13] A. Bakeer, A. Chub, D. Vinnikov, and A. Rosin, "Wide input voltage range operation of the series resonant DC-DC converter with bridgeless boost rectifier," *Energies*, vol. 13, no. 16, Aug. 2020. Art. no. 4220.

- [14] T. LaBella, W. Yu, J. Lai, M. Senesky, and D. Anderson, "A bidirectional-switch-based wide-input range high-efficiency isolated resonant converter for photovoltaic applications," *IEEE Trans. Power Electron.*, vol. 29, no. 7, pp. 3473–3484, Jul. 2014.
- [15] J.-P. Vandaelac and P. D. Ziogas, "A DC to DC PWM series resonant converter operated at resonant frequency," *IEEE Trans. Ind. Electron.*, vol. 35, no. 3, pp. 451–460, Aug. 1988.
- [16] V. Sidorov, A. Chub, and D. Vinnikov, "Performance improvement of PWM control methods for voltage step-down in series resonant DC-DC converters," *Energies*, vol. 13, Sept. 2020. Art. no. 4569.
- [17] E.-H. Kim and B.-H. Kwon, "Zero-voltage- and zero-current-switching full-bridge converter with secondary resonance," *IEEE Trans. Ind. Electron.*, vol. 57, no. 3, pp. 1017–1025, Mar. 2010.
- [18] Y. V. Singh, K. Viswanathan, R. Naik, J. A. Sabate, and R. Lai, "Analysis and control of phase-shifted series resonant converter operating in discontinuous mode," in *Proc. APEC*, Long Beach, CA, 2013, pp. 2092–2097.
- [19] M. Pahlevani, S. Pan, and P. Jain, "A hybrid phase-shift modulation technique for DC/DC converters with a wide range of operating conditions," *IEEE Trans. Ind. Electron.*, vol. 63, no. 12, pp. 7498–7510, Dec. 2016.
- [20] X. Sun, X. Li, Y. Shen, B. Wang, and X. Guo, "Dual-Bridge LLC resonant converter with fixed-frequency PWM control for wide input applications," *IEEE Trans. Power Electron.*, vol. 32, no. 1, pp. 69–80, Jan. 2017.
- [21] G. Moschopoulos and P. Jain, "A series-resonant DC/DC converter with asymmetrical PWM and synchronous rectification," in *Proc. PESC*, Galway, Ireland, vol. 3, pp. 1522–1527, 2000.
- [22] K. Ali, P. Das, and S. K. Panda, "Analysis and design of APWM half-bridge series resonant converter with magnetizing current assisted ZVS," *IEEE Trans. Ind. Electron.*, vol. 64, no. 3, pp. 1993–2003, Mar. 2017.
- [23] D. Vinnikov, A. Chub, O. Korkh, and M. Malinowski, "Fault-Tolerant bidirectional series resonant DC-DC converter with minimum number of components," in *Proc. IEEE ECCE*, Baltimore (MD), USA, Sep. 29–Oct 3, 2019, pp. 1359–1363.
- [24] D. Vinnikov, A. Chub, E. Liivik, and I. Roasto, "High-Performance quasi-z-source series resonant DC-DC converter for photovoltaic module-level power electronics applications," *IEEE Trans. Power Electron.*, vol. 32, no. 5, pp. 3634–3650, May 2017.
- [25] B. Luan, S. Hu, Y. Zhang, and X. Li, "Steady-state analysis of a series resonant converter with modified PWM control," in *Proc. 12th IEEE Conf. Ind. Electron. Appl. (ICIEA)*, Siem Reap, 2017, pp. 1143–1148.
- [26] S. C. Wong, A. D. Brown, Y. S. Lee, and S. W. Ng, "Parasitic losses modeling of a series resonant converter circuit," in *Proc. IEEE Int. Symp. Circuits Syst. (ISCAS)*, vol. 2, Hong Kong, 1997, pp. 921–924.
- [27] D. Graovac, M. Purschel, and A. Kiep, "MOSFET power losses calculation using the data-sheet parameters," *Infineon Application Note*, Jul., 2006. Accessed: 7 July 2020. [Online] Available: <https://application-notes.digchip.com/070/70-41484.pdf>
- [28] K. Venkatachalam, C. R. Sullivan, T. Abdallah, and H. Tacca, "Accurate prediction of ferrite core loss with nonsinusoidal waveforms using only steinmetz parameters," in *Proc. IEEE Workshop Comput. Power Electron.*, Mayaguez, Puerto Rico, USA, 2002, pp. 36–41.
- [29] Product specifications. Core RM14/I, Ferroxcube a YAGEO company, 2016. Accessed: 7 July 2020. [Online] Available: https://www.ferroxcube.com/upload/media/product/file/Pr_ds/RM14_I.pdf
- [30] Data sheet. "Material specifications 3C95," *Ferroxcube A YAGEO Company*, Oct. 2015. Accessed: 7 July 2020. Online: Available <https://www.ferroxcube.com/upload/media/product/file/MDS/3c95.pdf>



VADIM SIDOROV (Student Member, IEEE) was born in Kazakhstan in 1995. He received the B.Sc. and M.Sc. degrees in power electronics from Novosibirsk State Technical University, Novosibirsk, Russia, in 2017 and 2019, respectively. He is currently working toward the Ph.D. degree with Power Electronics Group, Tallinn University of Technology, Tallinn, Estonia. His research interests include power electronics systems, dc–dc converters, series resonant converters, dc–ac inverters, and electric drive systems.



ANDRII CHUB (Senior Member, IEEE) was born in Chernihiv, Ukraine, in 1987. He received the B.Sc. and M.Sc. degrees in electronic systems from Chernihiv State Technological University, Ukraine, in 2008 and 2009, respectively, and the Ph.D. degree in electrical engineering from the Tallinn University of Technology, Estonia, in 2016.

He is a Senior Researcher with the Power Electronics Group, Department of Electrical Power Engineering and Mechatronics, Tallinn University of Technology. He was a Visiting Research Fellow with Kiel University, Kiel, Germany, in 2017, and a Postdoctoral Researcher with Federico Santa Maria Technical University, Valparaíso, Chile, between 2018 and 2019. He has coauthored more than 100 papers and a book chapter on power electronics and applications, and holds several patents and utility models. He was the recipient of numerous best paper awards at the IEEE conferences and the 2018 IES Best Conference Paper Award. His research interests include dc–dc converters, dc microgrids, renewable energy conversion systems for energy-efficient buildings, fault tolerance, and reliability of power electronic systems.

He is an Associate Editor for the IEEE JOURNAL OF EMERGING AND SELECTED TOPICS IN INDUSTRIAL ELECTRONICS.



DMITRI VINNIKOV (Senior Member, IEEE) was born in Tallinn, Estonia, in 1976. He received the Dipl.Eng., M.Sc., and Dr.Sc.techn. degrees in electrical engineering from the Tallinn University of Technology, Tallinn, Estonia, in 1999, 2001, and 2005, respectively.

He is currently a Research Professor and the Head of the Power Electronics Group, Department of Electrical Power Engineering and Mechatronics, Tallinn University of Technology, and a Guest Researcher with the Institute of Industrial Electronics and Electrical Engineering, Riga Technical University Riga, Latvia. He is the CTO and Cofounder of Ubik Solutions LLC—Estonian start-up company dedicated to innovative and smart power electronics for renewable energy systems. He is one of the Founders and Leading Researchers of ZEBE—Estonian Centre of Excellence for zero energy and resource efficient smart buildings and districts. He has authored or coauthored two books, five monographs, and one book chapter, as well as more than 300 published papers on power converter design and development, and is the holder of numerous patents and utility models in this field. His research interests include applied design of power electronic converters and control systems, renewable energy conversion systems (photovoltaic and wind), impedance-source power converters, and the implementation of wide bandgap power semiconductors.

He is a Chair of the IES/PELS Joint Societies Chapter of the IEEE Estonia Section.



ABUALKASIM BAKEER (Student Member, IEEE) was born in Qena, Egypt, in 1990. He received the B.Sc. and M.Sc. (Hons.) degrees in electrical engineering from Aswan University, Aswan, Egypt, in 2012 and 2017, respectively. Since September 2019, he has been working toward the Ph.D. degree with the Department of Electrical Power Engineering and Mechatronics, Tallinn University of Technology, Estonia. Since 2014, he has been with Electrical Engineering Department, Faculty of Engineering, Aswan

University, first as a Demonstrator, and then as an Assistant Lecturer in 2017. He is the author or coauthor of more than 15 scientific papers. His main research interests include dc–dc converters, fault diagnosis and fault tolerance, ac drives, impedance-source power converters, and model predictive control. He was a Reviewer in the IEEE TRANSACTION ON INDUSTRIAL ELECTRONICS, the IEEE TRANSACTION ON INDUSTRIAL INFORMATICS, and the IEEE JOURNAL OF EMERGING AND SELECTED TOPICS IN INDUSTRIAL ELECTRONICS.